JACS
JOURNAL OF THE AMERICAN CHEMICAL SOCIETY
pubs.acs.org/JACS

Article

Regioswitchable Bingel Bis-Functionalization of Fullerene C_{70} via Supramolecular Masks

Valentina Iannace, Clara Sabrià, Youzhi Xu, Max von Delius, Inhar Imaz, Daniel Maspoch, Ferran Feixas,* and Xavi Ribas*

Cite This: J. Am. Chem. Soc. 2024, 146, 5186−5194

Read Online

ACCESS | Metrics & More | Article Recommendations | Supporting Information

ABSTRACT: Isomer-pure functionalized fullerenes are required to boost the development of fullerene chemistry in any field, but their multiple functionalization renders a mixture of regioisomers that are very difficult to purify by chromatography. For the specific case of C_{70}, its nonspherical geometry makes its regioselective functionalization more challenging than that of spherical C_{60}. In this work, the supramolecular mask approach is applied for the first time to C_{70}, which is encapsulated in two different nanocapsules to achieve the Bingel bis-cyclopropanation at α-bonds of opposite poles. Based on the tetragonal prismatic geometry imposed by the smaller supramolecular mask tested, the obtained major bis-adduct is completely reversed (major 5 o'clock) compared to bare C_{70} functionalization (major 2 o'clock). Moreover, by further restricting the accessibility of C_{70} using a three-shell Matryoshka mask and dibenzyl-bromomalonate, a single regiospecific 2 o'clock bis-isomer is obtained, owing to the perfect complementarity of the mask and the addend steric properties. The outcome of the reactions is fully explained at the molecular level by means of a thorough molecular dynamics (MD) study of the accessibility of the α-bonds to produce the different bis-adducts.

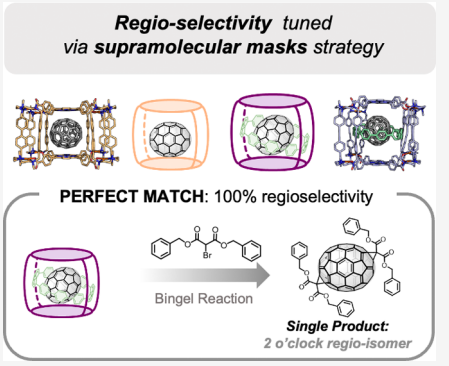

INTRODUCTION

Fullerenes are privileged electron transporting materials (ETM) widely used in organic solar cells (OSCs) and perovskite solar cells (PSCs).[1] The high electron mobilities and 3D spheroidal character of fullerenes result in robust charge delocalization and high power conversion efficiency (PCE). However, only easily accessible and solution-processable monofunctionalized PCBM ([6,6]-phenyl-butyric acid methyl ester) derivatives of C_{60} and C_{70} are typically considered as viable ETM contenders.[2−6] As a consequence, there is a serious lack of diversity in fullerene-based ETM for PSCs, a clear drawback in the development of new generation cells. In particular, pure polyfunctionalized fullerenes are highly desirable to boost the development of fullerene-based materials,[3,6,7] but they are practically inaccessible due to the formation of intractable mixtures of tens of regioisomers when there are two or more addends on the fullerene (Figure 1A).[8−11] Very few strategies, reported in the 1990s, exist to overcome this resounding limitation: the "tether-directed remote functionalization" strategy for the synthesis of polycyclopropanated adducts (Bingel-Hirsch) under regiocontrol (Figure 1B)[12−15] and the "orthogonal transposition" for the production of equatorial tetrakis-cyclopropanated-C_{60} adducts (Figure 1C).[16,17] Recently, supramolecular masks have emerged as a valid way to have practical access to isomerically pure polyfunctionalized C_{60}.[18] Pioneered by our group, this approach consists of designing supramolecular hosts with a high affinity for fullerenes and then subjecting the resulting host−guest adduct to fullerene functionalization conditions, allowing the chemo- and regioselective derivatization only at the exposed surface of the fullerene left by the supramolecular mask. In this manner, we reported the sequential synthesis of bis-, tris-, or tetrakis-equatorial adducts in a selective manner using Bingel cyclopropanated addends (Figure 1D)[19] or acene cycloadded addends.[20] Also recently, a supramolecular three-shell Matryoshka-like complex featuring C_{60} encapsulation was reported and used as a mask to deliver *trans*-3 bis-adducts[21] and [2]catenanes incorporating both C_{60} and [10]CPP nanohoop (Figure 1E).[22]

Less is known about the control of the mono- and polyfunctionalization of C_{70}.[23] In contrast to a single possible isomer for monosubstituted-C_{60} due to its spherical geometry, there can exist eight different monosubstituted isomers of C_{70} due to its oval-shaped ellipsoidal geometry.[24,25] Four of these bonds are located at the junction between two six-membered rings (6,6′ bonds), and the other four are at the junction between a six- and a five-membered ring (6,5′ bonds).[26,27]

Received: September 30, 2023
Revised: January 13, 2024
Accepted: January 16, 2024
Published: February 5, 2024

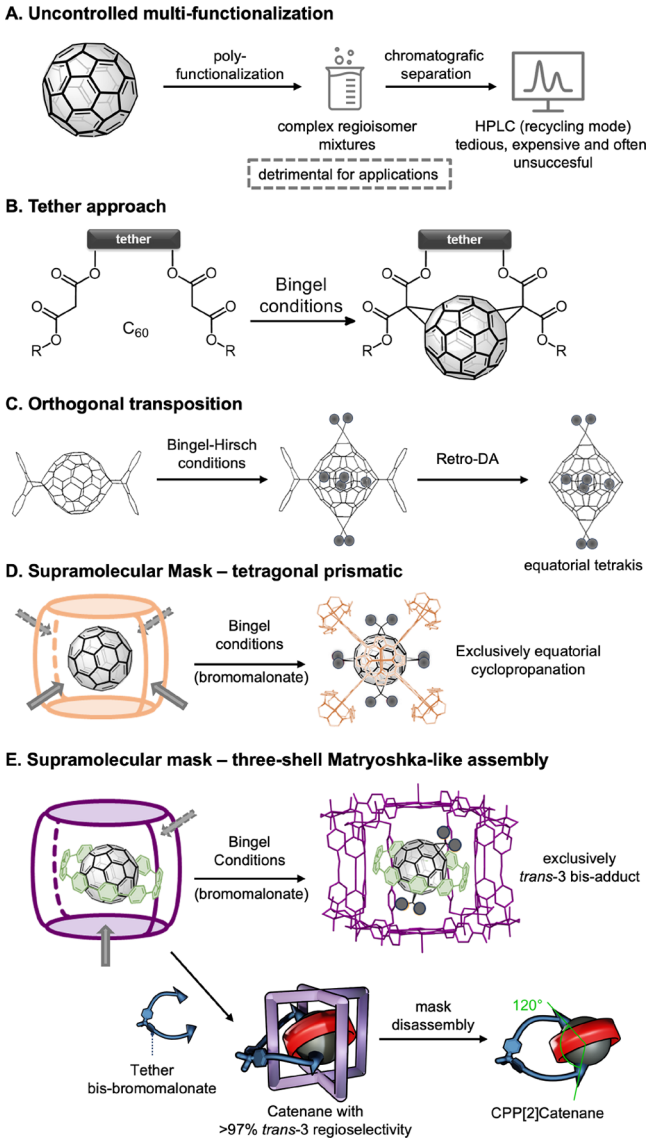

Figure 1. Current regio-functionalization strategies of fullerene C_{60}.

Additionally, four types of (6,6′) bonds (α, β, γ, and δ) can render mixtures, as in the case of monosubstituted-C_{70} with PCBM ([6,6]-phenyl butyric acid methyl ester), where α and β addends can be obtained.[28,29] Consequently, regioselective bis-functionalization of C_{70} entails much higher complexity than C_{60}. Bingel regiofunctionalization is chosen as a way to minimize the number of isomers formed during the first addition step since it shows a strong preference for the (6,6′) α-type bonds due to their highly pyramidalized C_{sp^2} atoms (Figure 2A).[26,27,30] Hence, after the first addend addition on an α-bond on one pole of C_{70}, the bis-adduct formation would preferentially occur at the five reactive (6,6′) α-bonds of the second pole.[26,27] If the malonate addend is symmetric, then bis addition to α-type bonds on opposite poles yields three constitutionally isomeric bis-fullerene Bingel adducts, named 12 o'clock, 2 o'clock, or 5 o'clock (Figure 2B). These regioisomers present characteristic UV−vis spectra that do not depend on the type of adduct but on the regioisomer nature.[26,27]

Performing Bingel functionalization using standard conditions (bromomalonate, DBU, toluene, 25 °C) yields a

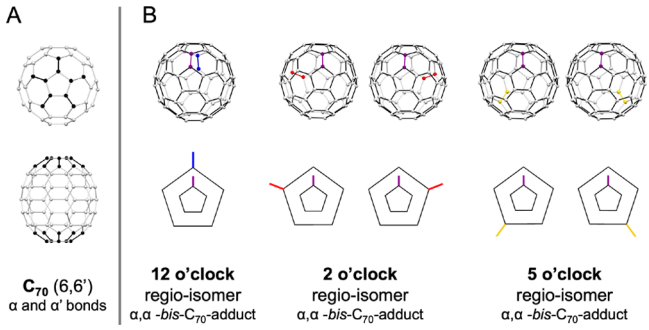

Figure 2. (A) α and α' (6,6′) bonds of C_{70}. (B) The three possible regioisomers of a bis-α,α-C_{70}-adduct (Schlegel diagram using the Newman-type projection, and with the C_{70} core viewed along the C_5 axis passing through the proximal (small) and distal (large) pentagons at the opposite poles of the fullerene).

mixture of Bingel bis-C_{70} adducts in an approximate ratio of 2.8:6.2:1 for 12 o'clock:2 o'clock:5 o'clock.[26] Tether-directed strategies have also been used on C_{70} to obtain controlled regioselectivity of bis regioisomers.[31,32] Regarding its poly-functionalization, a single C_2-symmetrical isomer of the tetrakis-Bingel-C_{70}, featuring a functionalized α and β bond at each pole, has been reported using bromomalonate/DBU/CCl_4/25 °C.[27] Moreover, polychlorination under very harsh conditions also allows for a controlled regioisomeric outcome to obtain $C_{70}Cl_{26}$ and subsequent rearrangements, as described by Troyanov and co-workers.[33]

No example of the use of supramolecular masks for controlling the regiofunctionalization of C_{70} has been reported, in spite of a significant number of reports describing the enhanced affinity of a specific host for C_{70} over C_{60}.[34−43] In this work, we challenge the regio-control ability of supramolecular masks by performing the Bingel bis-cyclopropanation reaction on C_{70} upon encapsulation in a tetragonal prismatic nanocapsule,[44] i.e., (C_{70}⊂**4**·$(BArF)_8$), and in a three-shell Matryoshka-like complex (C_{70}⊂[10]CPP⊂**6**·$(BArF)_8$).[21] We explored a series of four symmetrical bromomalonates differing in steric bulk to determine the limits of the mask strategy. Using nanocapsule **4**·$(BArF)_8$, we obtain the bis-C_{70}-adduct in a reversed ratio (5 o'clock major) compared to bulk functionalization (2 o'clock major), although overfunctionalization is not prevented. On the other hand, in the case of the three-shell C_{70}-Matryoshka-like complex, overfunctionalization is completely avoided, and a perfect match between the sterics of the nanocapsule structure and addend was found using dibenzyl-bromomalonate (**Bn**), exclusively obtaining the 2 o'clock regioisomer with ideal regioselectivity. In addition, MD simulations are successfully used to rationalize the experimental regioselectivity. Altogether, the supramolecular mask strategy is confirmed as a valuable tool for the synthesis of pure regioisomer-functionalized C_{70}-fullerene for future dedicated applications.

RESULTS AND DISCUSSION

Functionalization of Bare C_{70}. We started this study by reproducing the reported functionalization of bare C_{70} as a reference experiment in which no restrictions are imposed on regioselectivity.[26] The reaction was performed at room temperature in *o*-dichlorobenzene (*o*-DCB):DMSO (2:1) using Na_2CO_3 as a base), and using bromomalonates of different steric bulk: diethyl-bromomalonate (**Et**), di-isoprop-

https://doi.org/10.1021/jacs.3c10808
J. Am. Chem. Soc. 2024, 146, 5186−5194

yl-bromomalonate (*i*Pr), di-tert-butyl-bromomalonate (*t*Bu), and dibenzyl-bromomalonate (Bn). The reaction was stopped when the bis-adduct formation was maximized (20−60 min), although bare C_{70}, monoadduct, and polyadducts (>tris) were also found in the final mixture (TLC monitoring in DCM) (Figure 3A). Column chromatography was performed to

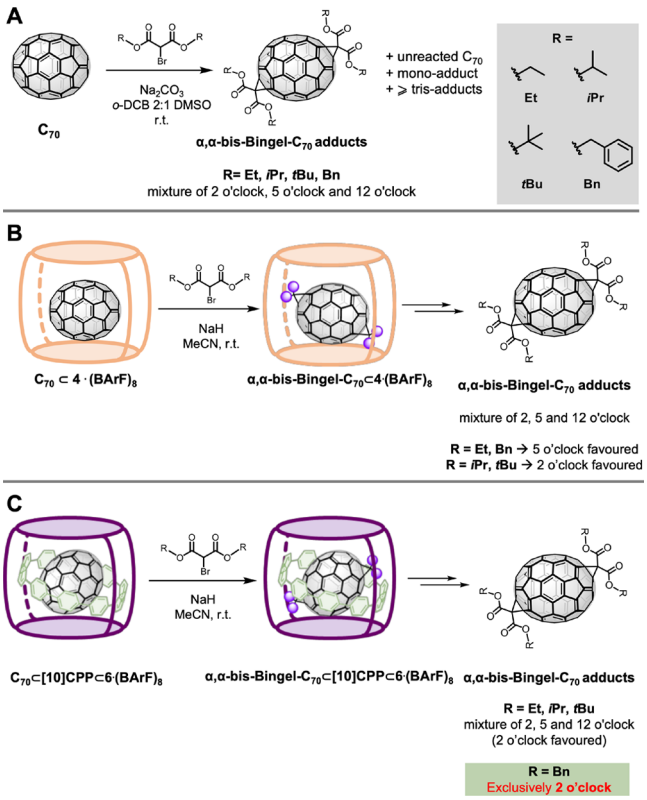

Figure 3. General procedures for the functionalization of C_{70}. (A) Using bare C_{70}; (B) using C_{70}⊂**4**·$(BArF)_8$; and (C) using C_{70}⊂[10]-CPP⊂**6**·$(BArF)_8$.

collect the bis-adducts from a mixture also containing mono-, tris-, and higher adducts, which accounted for a low ∼5% yield of bis-adducts. Subsequent preparative TLC allowed isolating each bis-adduct, which was identified by the characteristic UV−vis spectra. In all cases, we obtained the 2 o'clock regioisomer as the major product (relative ratio 68−69%) and the 12 and 5 o'clock regioisomers in smaller amounts (relative ratios 10−21%).

Since it was reported that [10]CPP can impart some regioselectivity to C_{60},[45,46] we prepared the supramolecular assembly C_{70}⊂[10]CPP and exposed it to Bingel reaction conditions using the dibenzyl-bromomalonate. The obtained regioisomer ratios (2.0:6.8:1.2 ratio of 12:2:5 o'clock) were similar to those found for bare C_{70}, thus indicating that the [10]CPP nanohoop does not impart any significant degree of control to the regioselectivity of C_{70} functionalization.

The above preliminary experiments clearly showed the intrinsic challenges in controlling the regioselectivity and the urgent need to a) prevent the polyfunctionalization and b) improve the regioselectivity of the reaction.

Supramolecular Mask Strategy. C_{70} was encapsulated in a tetragonal prismatic Pd-based nanocapsule **4**·$(BArF)_8$ (Figure 4), which presented a high affinity for fullerene C_{70} (K_a > 10^8 M^{-1}) as previously reported by our group.[44] The

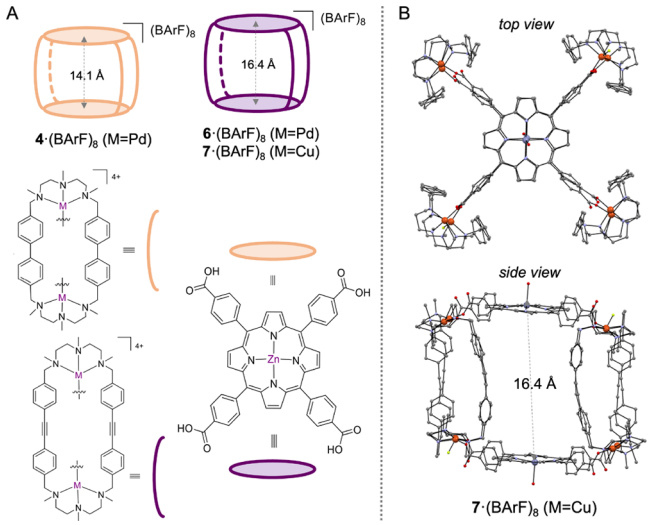

Figure 4. (A) Composition of Pd-based nanocapsules **4**·$(BArF)_8$ and **6**·$(BArF)_8$ and the Cu-based **7**·$(BArF)_8$ nanocapsule (isostructural to **6**). (B) Crystal structure of **7**·$(BArF)_8$ obtained by synchrotron radiation, top and side views.

encapsulation was performed analogously to the reported one (MeCN 1:9 toluene, 24 h, r.t.), and the formation of C_{70}⊂**4**·$(BArF)_8$ was confirmed by HR-MS (ESI-QTOF) (Figure S62).

With the host−guest complex C_{70}⊂**4**·$(BArF)_8$ in our hands, it was exposed to the Bingel reaction conditions using MeCN as the solvent and NaH as the base. By HR-MS monitoring (Figures S54−S57), we found that the functionalization process was slowed down compared to bare C_{70}, although still a 1:1 mixture of tris- and tetrakis-adducts was obtained in 24 h. Since the focus of interest was the bis-adduct regioselectivity, we optimized the reaction conditions to obtain the bis-adducts as major products (yields in the range of 13−40%, depending on the malonate; 3 to 4 h) when a maximum of 4 equiv of the bromomalonates was used. The general procedure to obtain the targeted product required the disassembly of the nanocapsule with triflic acid to release the adducts (see the workflow in Figure S18). Then, the three regioisomers were separated by TLC and quantified by HPLC (see the ratios in Figure 5B). In most cases, the ratio of the 12 o'clock regioisomer was reduced (the special case of the bis-*t*Bu-C_{70}-adduct is explained by MD simulations, see below), whereas the ratio of the 5 o'clock regioisomer was clearly improved. Indeed, for the diethyl- (**Et**) and dibenzyl- (**Bn**) bromomalonate, the favored product switched from 2 o'clock to 5 o'clock regioisomers up to a ratio of 42:58 for **Et** and a remarkable ratio of 23:73 for **Bn** (Figure 5B).

To restrict the regioselectivity even further and to gain control over the number of additions ("itero-selectivity"),[47] **C_{70}-Matryoshka**, i.e., C_{70}⊂[10]CPP⊂**6**·$(BArF)_8$, was synthesized. We initially prepared the C_{70}⊂[10]CPP assembly, and then it was accommodated in the larger nanocapsule **6**·$(BArF)_8$, taking inspiration from our previous work with C_{60}.[21] The structure of the Cu-based **7**·$(BArF)_8$ empty nanocapsule (isostructural to the Pd-based **6**·$(BArF)_8$) was elucidated by synchrotron radiation (Figure 4B). As expected, it featured a tetragonal prismatic capsule with a suitable large cavity ($d_{ZnPorph\cdots ZnPorph}$ = 16.46 Å) to host the C_{70}⊂[10]CPP guest. The three-shell **C_{70}-Matryoshka** was thus obtained by mixing both C_{70}⊂[10]CPP and **6**·$(BArF)_8$ nanocapsules in a mixture of MeCN:DCM (1:1) at room temperature overnight. Its full

https://doi.org/10.1021/jacs.3c10808
J. Am. Chem. Soc. 2024, 146, 5186−5194

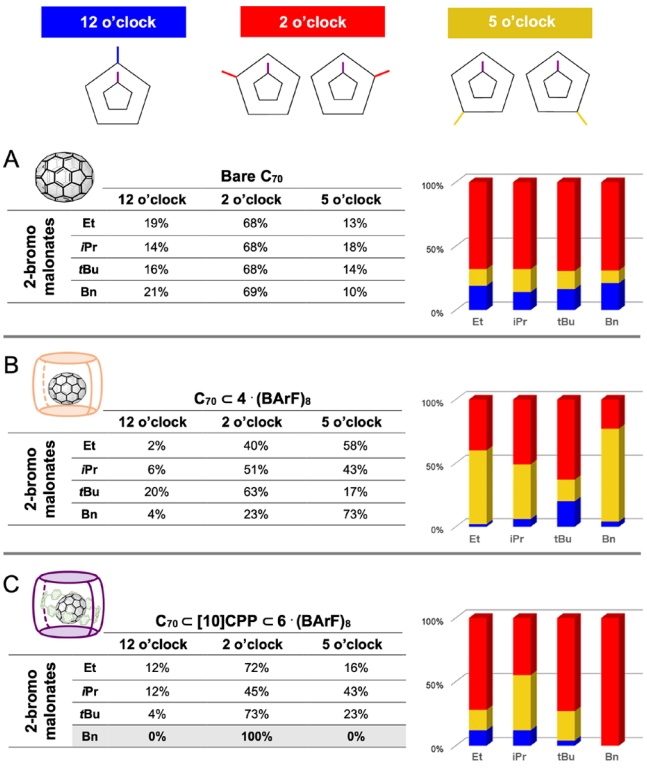

Figure 5. Experimental results obtained with the four bromomalonates (**Et**, *i***Pr**, *t***Bu**, and **Bn**) for (A) bare C_{70}, (B) using nanocapsule **4**·$(BArF)_8$, and (C) **C_{70}-Matryoshka**.

formation was confirmed by HRMS (ESI-QTOF) (Figure S67). The single crystal structure of C_{70}⊂[10]CPP⊂**6**·$(BArF)_8$ was repeatedly attempted at the synchrotron but was unsuccessful, presumably due to the intrinsic dynamics of the three-shell **C_{70}-Matryoshka** (see MD simulations below).

Remarkably, when the three-shell **C_{70}-Matryoshka** was exposed to the Bingel reaction conditions in MeCN, we observed only the appearance of bis-adduct peaks by HRMS monitoring (see Figures S58−S61). Identical results were seen when an excess of bromomalonate (8−10 equiv) and base NaH (8−10 equiv) were used for 24 h at room temperature. This observation clearly indicated that our three-shell supramolecular mask prevents the polyfunctionalization over bis-adducts. The removal of the encapsulated bis-C_{70}-adduct was achieved by the addition of an excess of fullerene C_{60} or C_{70}, which have a higher affinity than bis-functionalized-C_{70}. In this way, the bis-adducts were released in chloroform and a reusable **C_{60}-** or **C_{70}-Matryoshka** was created (see the workflow in Figure S24). For all the bromomalonates used (**Et**, *i***Pr**, *t***Bu**, and **Bn**), bis-adducts were solely obtained in a yield ranging from 29 to 43%. The bis-α,α-regioisomer were separated by TLC and quantified by HPLC. Comparing the ratios of bis-α,α-regioisomers obtained using the **C_{70}-Matryoshka** mask (Figure 5C) with the ones synthesized using the supramolecular mask **4**·$(BArF)_8$ (Figure 5B), the ratio for 12 o'clock was again reduced. On the contrary, the three-shell mask was not favoring the 5 o'clock regioisomer in any case, and 2 o'clock was the major regioisomer. Remarkably, the steric bulk of the malonate is key to achieving a proper match, and in the case of the dibenzyl bromomalonate (**Bn**), the 2 o'clock regioisomer was obtained exclusively with an ideal regioselectivity. To our knowledge, this is the first reported pure-isomer bis-Bingel functionalization of C_{70}.

Attempts to perform the reaction using a catalytic amount of C_{70}⊂[10]CPP⊂[**6**·$(BArF)_8$] and excess of C_{70} were made in pure MeCN, but very low yields of 2-o'clock bis-adduct were obtained. Evident nanocapsule decomposition due to a large excess of base hampered any turnover, albeit only the 2-o'clock bis-adduct was formed because the reaction occurred exclusively in the confined space of the Matryoshka.

Molecular Dynamics (MD) Simulations to Unravel Fullerene Accessibility. MD simulations for all cases were performed to rationalize the molecular basis of the observed experimental ratios between the bis-adduct regioisomers using both supramolecular masks. Our previous work showed that unfunctionalized C_{70} horizontally freely rotates inside the **4**·$(BArF)_8$, sampling multiple orientations.[48] This indicates that fullerene rotation is not restricted by the nanocapsule and that the α-bonds of both poles are equally exposed. Here, we hypothesized that both the supramolecular mask and the interactions established by the monoadducts with the nanocapsule will precisely control the dynamics of the fullerene and the accessibility of the α-bonds to achieve the regioselective formation of bis-adducts.

All MD simulations were performed starting from monoadduct-C_{70} placed inside the nanocapsule using either **4**·$(BArF)_8$, i.e., mono-C_{70}⊂**4**·$(BArF)_8$, or the **C_{70}-Matryoshka** complex, i.e., mono-C_{70}⊂[10]CPP⊂**6**·$(BArF)_8$, performing five replicates of 0.5 μs for each system. Since the bis-adduct formation must take place through one of the four windows of the nanocapsule, the accessibility of the three different bonds of the mono-C_{70} that will deliver the 2 o'clock, 5 o'clock, and 12 o'clock bis-adducts has been assessed using different criteria: criterion A) monitoring the distance between each α-bond and the porphyrins (nanocapsule centrality); criterion B) focusing on the proximity of each α-bond to the center of the window of the nanocapsule (window proximity); and Criterion C) in the case of the **C_{70}-Matryoshka** complex, focusing on their distance from the [10]CPP ring (blocked by the nanohoop) (further details in Figures 6 and 8 and the SI). Altogether, we considered that the bond that is placed farther from both porphyrins, closer to the center of the window, and is less shielded by the [10]CPP ring will be the most accessible. The position with more accessibility (less shielded by the supramolecular mask) will probably be the one that reacts more, so the yield of the corresponding bis-adduct would be higher. Additionally, each bis-adduct has been simulated to study its conformation inside the corresponding mask and to estimate its binding free energy (ΔG_{bind}). We have conducted a comprehensive MD study with the two masks and the four bromomalonates (complete analysis in section 6 in the SI), although we focus our discussion on the dibenzyl-malonate addend since it shows the best steric complementarity among host and guest and therefore the effect of each supramolecular mask is maximized.

In the case of the (6,6′) α-bond mono-di-benzylmalonate-C_{70} adduct encapsulated in nanocapsule **4**·$(BArF)_8$, we have specifically explored the accessibility to the α-bonds of the second pole through the gates of the mask. By collectively analyzing all MD replicates, we observed that the 5 o'clock position followed by 2 o'clock are the most accessible considering criteria A and B (Figure 6). The visual inspection of MD simulations revealed that the encapsulated mono-di-benzylmalonate-C_{70} adduct scans two major orientations inside

https://doi.org/10.1021/jacs.3c10808
J. Am. Chem. Soc. 2024, 146, 5186−5194

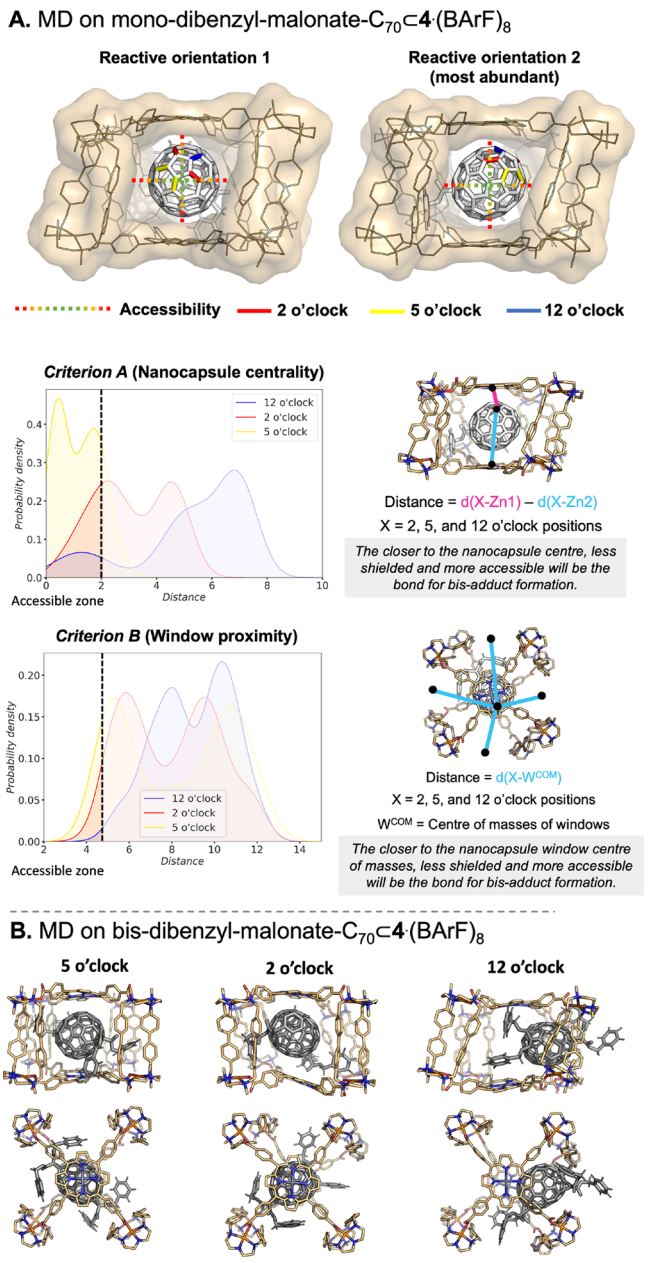

Figure 6. (A) MD studies on mono-di-benzyl-malonate-C_{70}⊂**4**·$(BArF)_8$ and accessibility analysis using criteria A and B. Space-filling models of two representative structures are used to show the accessibility of the α-bonds. Probability density plots of criteria A and B obtained from five replicas of 500 ns of MD simulations (all distances are in Å) where X = 2, 5, and 12 o'clock centers of mass; Zn1 and Zn2 = the position of the zinc ions of the porphyrin rings; and W^{COM} = Centre of masses of nanocapsule windows. The thresholds of the accessible zones are determined based on nonmasked regions in the space filling models. (B) Representative structures of bis-dibenzyl-malonate-C_{70}⊂**4**·$(BArF)_8$ obtained from MD simulations.

the nanocapsule, showing reduced rotation compared to unfunctionalized C_{70} (Figure 6 and Videos S1 and S2).[48] In the most populated one, the dibenzylmalonate moiety is stabilized between two clips, fixing the orientation of C_{70} and exposing the opposite pole in the opposite window. In the second orientation, the malonate is stabilized by only one clip, with each phenyl moiety placed in the center of a different window, which makes the α-bonds accessible from the adjacent windows (Figure S73). In agreement with the distance criteria, in both orientations the 5 o'clock is the position located closer to the center of the nanocapsule window. The other two positions are less accessible in both orientations, which indicates that they are pointing more toward one porphyrin or shielded by the window clips. These results are in agreement with the experimental higher relative ratio of 5 o'clock (0.4:2.3:7.3 ratio for 12:2:5 o'clock).

The final 12, 2, and 5 o'clock bis-adducts were also simulated upon encapsulation, showing that the 5 o'clock bis-adduct indeed adopts the most stable complex with the cage with a binding energy of −77.5 kcal/mol (see Figure 6). For the 2 o'clock bis-adduct, a stable complex is also observed, with a relative binding energy of +0.9 kcal/mol with respect to the 5 o'clock. Finally, for the 12 o'clock adduct, it adopts a less stable off-centered stabilization at one of the gates of the nanocapsule, with a relative binding energy of +5.4 kcal/mol. Along with the accessibility studies, the less thermodynamically stable 12 o'clock bis-adduct is translated in a residual yield obtained experimentally, and the most stable 5 o'clock bis-adduct is the major regioisomer obtained.

An analogous predictive analysis is performed for the diethyl-malonate and diisopropyl-malonate addends, with results in agreement with the relative ratios experimentally observed (see Figures S74 and S75). On the contrary, the experimentally observed trend of enhanced formation of the 5 o'clock addend is absent for di-tert-butyl-malonate addends, since the major bis-adduct obtained is the 2 o'clock and the ratio distribution is very similar to the one obtained with bare C_{70} (Figure 5). MD simulations of mono-di-^{t}Bu-malonate-C_{70}⊂**4**·$(BArF)_8$ shed light on this result, since in three out of five replicates the mono-di-^{t}Bu-malonate-C_{70} adduct is displaced toward one of the entries of the nanocapsule (Figures 7 and S76). This conformation is equivalent to the

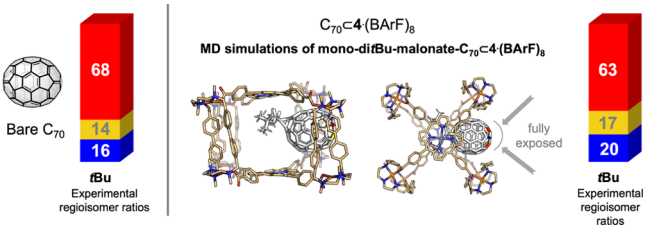

Figure 7. Comparative experimental regioisomer ratios found for bare C_{70} (left) and C_{70}⊂**4**·$(BArF)_8$ (right, along with the MD simulations of mono-di-^{t}Bu-malonate-C_{70}⊂**4**·$(BArF)_8$ predicting full exposure of the fullerene. Color code: blue (12 o'clock), red (2 o'clock), and yellow (5 o'clock).

functionalization of bare C_{70} since the nanocapsule cannot exhibit its mask action due to the almost complete exposure of the unfunctionalized pole of C_{70}.

We then analyzed the case of the mono-di-benzylmalonate-C_{70} adduct encapsulated in the Matryoshka assembly, i.e., mono-di-benzylmalonate-C_{70}⊂[10]CPP⊂**6**·$(BArF)_8$. Using criteria A and B, the most accessible position is 2 o'clock, which is the only bis-adduct obtained experimentally (Figure 8 and Videos S3 and S4). Since the [10]CPP ring is now present and may block the accessibility to C_{70}, we established criterion C, which accounts for the ability of [10]CPP to block 2, 5, and 12 o'clock positions (Figure 8). With criterion C, the accessible positions, not blocked by [10]CPP, are 12 o'clock

https://doi.org/10.1021/jacs.3c10808
J. Am. Chem. Soc. 2024, 146, 5186−5194

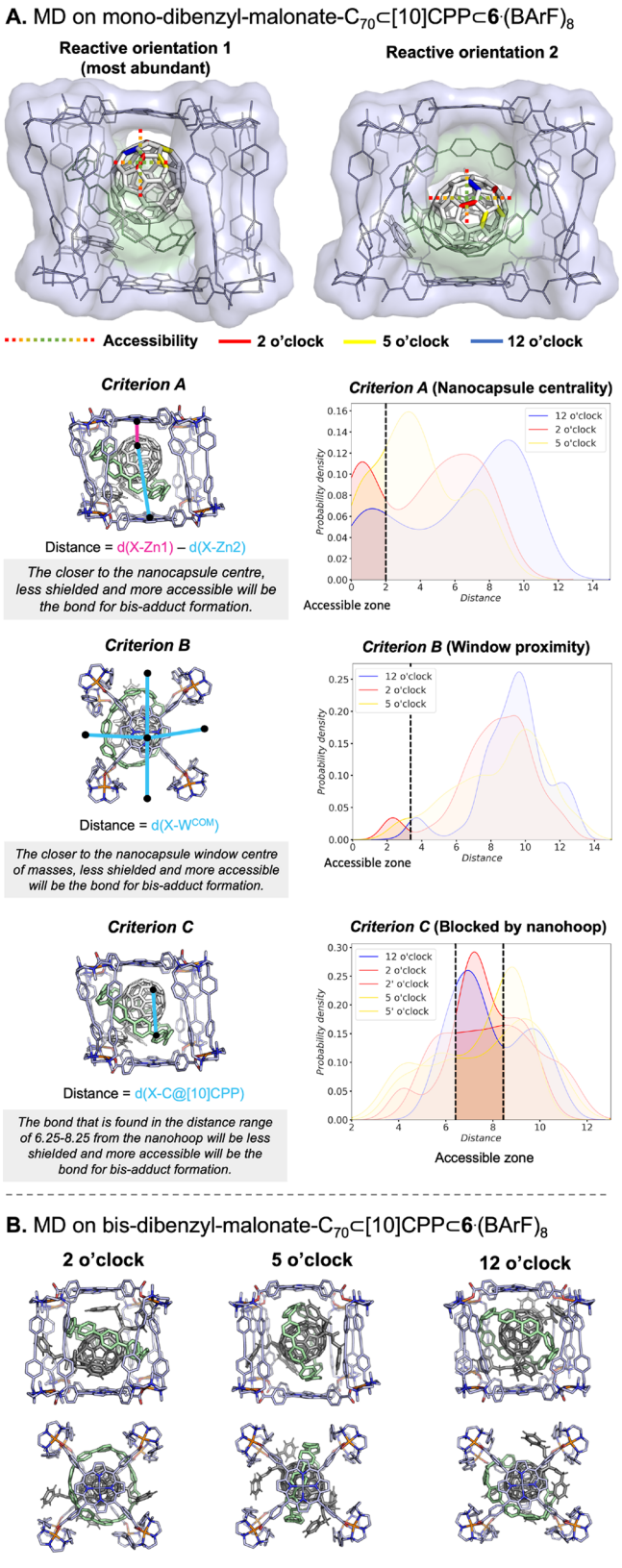

Figure 8. (A) MD studies on mono-di-benzyl-malonate-C_{70} ⊂[10]-CPP⊂**6**·$(BArF)_8$ and accessibility analysis using criteria A, B, and C. Space-filling models of two representative structures are used to show the accessibility of the α-bonds. Probability density plots of criteria A and B obtained from five replicas of 500 ns of MD simulations (all distances are in Å) where X = 2, 5, and 12 o'clock centers of mass; Zn1 and Zn2 are the positions of the zinc ions of the porphyrin rings; W^{COM} represents the centers of mass of nanocapsule windows; and C@[10]CPP is a carbon atom in the [10]CPP nanohoop. The thresholds of the accessible zones are determined based on nonmasked regions of the space-filling models. (B) Representative structures of bis-dibenzyl-malonate-C_{70}⊂[10]CPP⊂**6**·$(BArF)_8$ obtained from MD simulations.

and one of the 2 o'clocks. The visual inspection of MD simulations reveals that the supramolecular mask reduces the dynamicity of the mono-di-benzylmalonate-C_{70} adduct, which is anchored through a network of interactions between the dibenzylmalonate addend and the nanocapsule clips. In these orientations, the 12 o'clock regioisomer is always placed backward and the 2 o'clock is facing the gate of the nanocapsule **6**·$(BArF)_8$ (Figure 8A), thus the simulations clearly suggest that 2 o'clock is the most favored. Interestingly, both 5 o'clock positions are generally shielded by the nanohoop in [10]CPP⊂**6**·$(BArF)_8$, which may be key to reverting the regiofunctionalization trends observed in **4**·$(BArF)_8$.

Also analyzing the bis-dibenzyl-C_{70} adducts inside the three-shell Matryoshka complex, we observe that, in the case of the 5 o'clock regioisomer, the [10]CPP ring rotates and it is placed vertically with respect to the porphyrin planes. This state tenses the cage to higher Zn−Zn distances among nanocapsule **6**·$(BArF)_8$ ($d_{ZnPorph\cdots ZnPorph}$ > 18 Å), which renders this conformation highly unstable and residual. In contrast, for the 2 o'clock regioisomer, we observe a stable conformation in which one of the phenyl substituents of the addend establishes an interaction with the porphyrin and the other addend interacts with the phenyls of the clips (Figure 8B and Video S5). In addition, the average Zn···Zn distances are the same as those for the initial Matryoshka assembly, so the nanocapsule **6**·$(BArF)_8$ is likely not strained. This perfect match between the 2 o'clock bis-dibenzyl-C_{70} adduct and the [10]-CPP⊂nanocapsule allows for a favored accommodation and perfect 100% regioselectivity for the 2 o'clock regioisomer.

The MD analysis of most accessible bis-adducts with diethyl-malonate and diisopropyl-malonate addends utilizing criteria A, B, and C afforded the bis-adduct 2 o'clock as mainly favored, albeit 12 o'clock also appears to be favored in some of them (criterion C for diethyl-malonate and criterion A for diisopropyl-malonate) (Figures S78 and S79). The latter might be reflected in the experimental finding of 12% ratios of 12 o'clock in both cases (Figure 5C). On the other hand, the MD study of mono-di-^{t}Bu-malonate-C_{70}⊂[10]CPP⊂**6**·$(BArF)_8$ showed that in four out of five replicates the [10]CPP was placed vertically aligned inside the cavity of the nanocapsule, thus in a destabilizing mode caused by the bulkier ^{t}Bu groups (Figure S80). Moreover, the MD analysis of the corresponding bis-adducts also points toward destabilizing conformations. Experimentally, we do observe very similar ratios among the three possible bis-adducts as if no supramolecular mask was present. We hypothesize that the reaction could take place at the gates or outside the cavity of the nanocapsule; therefore, the mask effect is lost. The latter is indeed supported by the observation of empty nanocapsules by HR-MS at the same voltage as where the other malonates are fully encapsulated.

CONCLUSIONS

We have undertaken a comprehensive study of the use of supramolecular masks for taming the regioselectivity in the bis-

https://doi.org/10.1021/jacs.3c10808
J. Am. Chem. Soc. 2024, 146, 5186−5194

Bingel functionalization of C_{70}. Compared to bare C_{70}, where ~68% of the 2 o'clock bis-adduct for all bromomalonates explored is generally obtained, the use of nanocapsule **4**·$(BArF)_8$ as a mask affords a remarkable switch of regioselectivity toward 5 o'clock over 2 o'clock. In the specific case of dibenzyl-bromomalonate (**Bn**), a 23:73 ratio of 2 o'clock:5 o'clock is achieved. To further restrict the exposed C_{70}, the three-shell mask C_{70}⊂[10]CPP⊂ **6**·$(BArF)_8$ was synthesized. The **C_{70}-Matryoshka** gave us perfect control of the polyfunctionalization, obtaining just the bis-adduct and the 2 o'clock as favored regioisomers. Again, in the case of dibenzyl-bromomalonate (**Bn**), a great match between the structure of the nanocapsule and the blockage of the [10]CPP and the addend strikingly led to the exclusive formation of the 2 o'clock bis-adduct as a pure regioisomer. MD simulations supported all experimental findings, providing us with a deep understanding of the dynamic behavior of mono- and bis-adducts inside the mask. Both the supramolecular mask and the interactions established by the monoadducts with the nanocapsule precisely control the dynamics and accessibility of the fullerene for bis-functionalization. This work demonstrates that the supramolecular mask strategy can also be a powerful tool to obtain chemo-, itero-, and regioselectivity in the less-explored functionalization of C_{70}. By changing the type of mask and/or the type of addend, the regioselectivity can be tuned. This strategy could be useful for the challenging synthesis of isomer pure C_{70} adducts for future dedicated applications such as molecular electronics and solar cell design.

■ ASSOCIATED CONTENT

Supporting Information

The Supporting Information is available free of charge at https://pubs.acs.org/doi/10.1021/jacs.3c10808.

Materials, instrumentation, experimental procedures, spectroscopic and photophysical characterization of all compounds, and refs 22−36 (PDF)

Mono-di-benzyl-C_{70}⊂**4**·$(BArF)_8$ (reactive orientation 1) (MPG)

Mono-di-benzyl-C_{70}⊂**4**·$(BArF)_8$ (reactive orientation 2 - most abundant) (MPG)

Mono-di-benzyl-C_{70}⊂[10]CPP⊂**6**·$(BArF)_8$ (reactive orientation 1 - most abundant) (MPG)

Mono-di-benzyl-C_{70}⊂[10]CPP⊂**6**·$(BArF)_8$ (reactive orientation 2) (MPG)

MD simulation of bis-dibenzyl-C_{70}⊂[10]CPP⊂**6**·$(BArF)_8$ (2 o'clock regio-isomer) (MOV)

Accession Codes

CCDC 2286023 (**7**·$(BArF)_8$) contains the supplementary crystallographic data for this paper. These data can be obtained free of charge via www.ccdc.cam.ac.uk/data_request/cif, or by emailing data_request@ccdc.cam.ac.uk, or by contacting The Cambridge Crystallographic Data Centre, 12 Union Road, Cambridge CB2 1EZ, UK; fax: +44 1223 336033.

■ AUTHOR INFORMATION

Corresponding Authors

Ferran Feixas − *Institut de Química Computacional i Catàlisi (IQCC) and Departament de Química, Universitat de Girona, Campus Montilivi, 17003 Girona, Catalonia, Spain;* orcid.org/0000-0001-5147-0000; Email: ferran.feixas@udg.edu

Xavi Ribas − *Institut de Química Computacional i Catàlisi (IQCC) and Departament de Química, Universitat de Girona, Campus Montilivi, 17003 Girona, Catalonia, Spain;* orcid.org/0000-0002-2850-4409; Email: xavi.ribas@udg.edu

Authors

Valentina Iannace − *Institut de Química Computacional i Catàlisi (IQCC) and Departament de Química, Universitat de Girona, Campus Montilivi, 17003 Girona, Catalonia, Spain*

Clara Sabrià − *Institut de Química Computacional i Catàlisi (IQCC) and Departament de Química, Universitat de Girona, Campus Montilivi, 17003 Girona, Catalonia, Spain*

Youzhi Xu − *Institute of Organic Chemistry, University of Ulm, 89081 Ulm, Germany;* Present Address: (Y.X.) College of Chemistry and Molecular Sciences, Henan University, Kaifeng 475004, China

Max von Delius − *Institute of Organic Chemistry, University of Ulm, 89081 Ulm, Germany;* orcid.org/0000-0003-1852-2969

Inhar Imaz − *Catalan Institute of Nanoscience and Nanotechnology (ICN2), CSIC and The Barcelona Institute of Science and Technology, 08193 Bellaterra, Catalonia, Spain;* orcid.org/0000-0002-0278-1141

Daniel Maspoch − *Catalan Institute of Nanoscience and Nanotechnology (ICN2), CSIC and The Barcelona Institute of Science and Technology, 08193 Bellaterra, Catalonia, Spain; ICREA, 08010 Barcelona, Catalonia, Spain;* orcid.org/0000-0003-1325-9161

Complete contact information is available at: https://pubs.acs.org/10.1021/jacs.3c10808

Notes

The authors declare no competing financial interest.

■ ACKNOWLEDGMENTS

This work was supported by grants from MINECO-Spain (PID2019-104498GB-I00, PID2022-136970NB-I00, and TED2021-130573B-I00 to X.R.; RTI2018-101032-J100, RYC2020-029552-I and PID2022-141676NB-I00 to F.F.), Fundación Areces (RegioSolar project to X.R.), and Generalitat de Catalunya AGAUR (2021SGR00475 and 2021SGR00487). V.I. thanks MINECO for a FPI grant, and C.S. thanks UdG for a Ph.D. grant. We thank the QBIS-CAT research group and STR-UdG for technical support. We also are grateful for the ICREA-Academia award to X.R. M.v.D. acknowledges financial support by the Deutsche Forschungsgemeinschaft (DFG), projektnummer 182849149-SFB953 "Synthetic Carbon Allotropes" (project A7).

■ REFERENCES

(1) Collavini, S.; Delgado, J. L. Fullerenes: the stars of photovoltaics. *Sustainable Energy & Fuels* **2018**, *2*, 2480−2493.

(2) Umeyama, T.; Igarashi, K.; Sakamaki, D.; Seki, S.; Imahori, H. Unique cohesive nature of the β1-isomer of [70]PCBM fullerene on structures and photovoltaic performances of bulk heterojunction films with PffBT4T-2OD polymers. *Chem. Commun.* **2018**, *54*, 405−408.

(3) Zhang, F.; Shi, W.; Luo, J.; Pellet, N.; Yi, C.; Li, X.; Zhao, X.; Dennis, T. J. S.; Li, X.; Wang, S.; Xiao, Y.; Zakeeruddin, S. M.; Bi, D.; Grätzel, M. Isomer-Pure Bis-PCBM-Assisted Crystal Engineering of Perovskite Solar Cells Showing Excellent Efficiency and Stability. *Adv. Mater.* **2017**, *29*, 1606806.

(4) Umeyama, T.; Miyata, T.; Jakowetz, A. C.; Shibata, S.; Kurotobi, K.; Higashino, T.; Koganezawa, T.; Tsujimoto, M.; Gélinas, S.; Matsuda, W.; Seki, S.; Friend, R. H.; Imahori, H. Regioisomer effects of [70]fullerene mono-adduct acceptors in bulk heterojunction polymer solar cells. *Chem. Sci.* **2017**, *8*, 181−188.
(5) Chiang, C.-H.; Nazeeruddin, M. K.; Grätzel, M.; Wu, C.-G. The synergistic effect of H_2O and DMF towards stable and 20% efficiency inverted perovskite solar cells. *Energy Environ. Sci.* **2017**, *10*, 808−817.
(6) Lenes, M.; Wetzelaer, G.-J. A. H.; Kooistra, F. B.; Veenstra, S. C.; Hummelen, J. C.; Blom, P. W. M. Fullerene Bisadducts for Enhanced Open-Circuit Voltages and Efficiencies in Polymer Solar Cells. *Adv. Mater.* **2008**, *20*, 2116−2119.
(7) Umeyama, T.; Imahori, H. Isomer Effects of Fullerene Derivatives on Organic Photovoltaics and Perovskite Solar Cells. *Acc. Chem. Res.* **2019**, *52*, 2046−2055.
(8) Maxouti, K. L.; Hirsch, A. Sequential Tether-Directed Synthesis of Pentakis-Adducts of C_{60} with a Mixed [3:2] Octahedral Addition Pattern. *Eur. J. Org. Chem.* **2018**, *2018*, 2579−2586.
(9) Yan, W.; Seifermann, S. M.; Pierrat, P.; Bräse, S. Synthesis of highly functionalized C_{60} fullerene derivatives and their applications in material and life sciences. *Organic & Biomolecular Chemistry* **2015**, *13*, 25−54.
(10) Schwenninger, R.; Müller, T.; Kräutler, B. Concise Route to Symmetric Multiadducts of [60]Fullerene: Preparation of an Equatorial Tetraadduct by Orthogonal Transposition. *J. Am. Chem. Soc.* **1997**, *119*, 9317−9318.
(11) Isaacs, L.; Diederich, F.; Haldimann, R. F. Multiple Adducts of C_{60} by Tether-Directed Remote Functionalization and synthesis of soluble derivatives of new carbon allotropes Cn(60 + 5). *Helv. Chim. Acta* **1997**, *80*, 317−342.
(12) Maxouti, K. L.; Hirsch, A. Sequential Tether-Directed Synthesis of Pentakis-Adducts of C_{60} with a Mixed [3:2] Octahedral Addition Pattern. *Eur. J. Org. Chem.* **2018**, *2018*, 2579−2586.
(13) Isaacs, L.; Diederich, F.; Haldimann, R. F. Multiple Adducts of C_{60} by Tether-Directed Remote Functionalization and synthesis of soluble derivatives of new carbon allotropes Cn(60 + 5). *Helv. Chim. Acta* **1997**, *80*, 317−342.
(14) Ioannou, C. P.; Chronakis, N. The first one-pot synthesis of a chiral pentakis-adduct of C_{60} utilising an opened-structure malonate tether. *Chem. Commun.* **2013**, *49*, 10611−10613.
(15) Đorđevic, L.; Casimiro, L.; Demitri, N.; Baroncini, M.; Silvi, S.; Arcudi, F.; Credi, A.; Prato, M. Light-Controlled Regioselective Synthesis of Fullerene Bis-Adducts. *Angew. Chem., Int. Ed.* **2021**, *60*, 313−320.
(16) Schwenninger, R.; Müller, T.; Kräutler, B. Concise Route to Symmetric Multiadducts of [60]Fullerene: Preparation of an Equatorial Tetraadduct by Orthogonal Transposition. *J. Am. Chem. Soc.* **1997**, *119*, 9317−9318.
(17) Castro, E.; Azmani, K.; Garcia, A. H.; Aghabali, A.; Liu, S.; Metta-Magana, A. J.; Olmstead, M. M.; Rodríguez-Fortea, A.; Poblet, J. M.; Echegoyen, L. Unusual C_{2h}-Symmetric *trans*-1-(Bis-pyrrolidine)-tetra-malonate Hexa-Adducts of C_{60}: The Unexpected Regio- and Stereocontrol Mediated by Malonate-Pyrrolidine Interaction. *Chem.—Eur. J.* **2017**, *23*, 15937−15944.
(18) Lu, Z.; Heard, A. W.; Nitschke, J. R. The fullerene awakens. *Chem.* **2022**, *8*, 2907−2908.
(19) Fuertes-Espinosa, C.; García-Simón, C.; Pujals, M.; Garcia-Borràs, M.; Gómez, L.; Parella, T.; Juanhuix, J.; Imaz, I.; Maspoch, D.; Costas, M.; Ribas, X. Supramolecular Fullerene Sponges as Catalytic Masks for Regioselective Functionalization of C_{60}. *Chem.* **2020**, *6*, 169−186.
(20) Pujals, M.; Pèlachs, T.; Fuertes-Espinosa, C.; Parella, T.; Garcia-Borràs, M.; Ribas, X. Regioselective access to orthogonal Diels-Alder C_{60} bis-adducts and tris-heteroadducts via supramolecular mask strategy. *Cell Rep. Phys. Sci.* **2022**, *3*, 100992.
(21) Ubasart, E.; Borodin, O.; Fuertes-Espinosa, C.; Xu, Y.; García-Simón, C.; Gómez, L.; Juanhuix, J.; Gándara, F.; Imaz, I.; Maspoch, D.; von Delius, M.; Ribas, X. A three-shell supramolecular complex enables the symmetry-mismatched chemo- and regioselective bis-functionalization of C_{60}. *Nat. Chem.* **2021**, *13*, 420−427.
(22) Steudel, F. M.; Ubasart, E.; Leanza, L.; Pujals, M.; Parella, T.; Pavan, G. M.; Ribas, X.; von Delius, M. Synthesis of C_{60}/[10]CPP-Catenanes by Regioselective, Nanocapsule-Templated Bingel Bis-Addition. *Angew. Chem., Int. Ed.* **2023**, *62*, e202309393.
(23) Banerjee, R.; Chakraborty, D.; Jhang, W.-T.; Chan, Y.-T.; Mukherjee, P. S. Structural Switching of a Distorted Trigonal Metal-Organic Cage to a Tetragonal Cage and Singlet Oxygen Mediated Oxidations. *Angew. Chem., Int. Ed.* **2023**, *62*, No. e202305338.
(24) Bingel, C. Cyclopropanierung von Fullerenen. *Chem. Ber.* **1993**, *126*, 1957−1959.
(25) Bingel, C.; Schiffer, H. Biscyclopropanation of C_{70}. *Liebigs Ann.* **1995**, *1995*, 1551−1553.
(26) Herrmann, A.; Rüttimann, M.; Thilgen, C.; Diederich, F. Multiple Cyclopropanations of C_{70}. Synthesis and characterization of bis-, tris-, and tetrakis-adducts and chiroptical properties of bis-adducts with chiral addends, including a recommendation for the configurational description of fullerene derivatives with a chiral addition pattern. *Helv. Chim. Acta* **1995**, *78*, 1673−1704.
(27) Herrmann, A.; Rüttimann, M. W.; Gibtner, T.; Thilgen, C.; Diederich, F.; Mordasini, T.; Thiel, W. Achiral and Chiral Higher Adducts of C_{70} by Bingel Cyclopropanation. *Helv. Chim. Acta* **1999**, *82*, 261−289.
(28) Matsumoto, F.; Sumino, S.; Iwai, T.; Ito, T. Regioselectivity enhancement in synthesis of [70]fullerene derivatives by introduction of a branched structure. *Org. Biomol. Chem.* **2019**, *17*, 2629−2634.
(29) Vidal, S.; Izquierdo, M.; Filippone, S.; Fernández, I.; Akin, S.; Seo, J.-Y.; Zakeeruddin, S. M.; Grätzel, M.; Martín, N. Site-selective Synthesis of β-[70]PCBM-like Fullerenes: Efficient Application in Perovskite Solar Cells. *Chem.—Eur. J.* **2019**, *25*, 3224−3228.
(30) Thilgen, C.; Diederich, F. Structural Aspects of Fullerene ChemistryA Journey through Fullerene Chirality. *Chem. Rev.* **2006**, *106*, 5049−5135.
(31) Cerón, M. R.; Izquierdo, M.; Aghabali, A.; Valdez, J. A.; Ghiassi, K. B.; Olmstead, M. M.; Balch, A. L.; Wudl, F.; Echegoyen, L. Tethered Bisadducts of C_{60} and C_{70} with Addends on a Common Hexagonal Face and a 12-Membered Hole in the Fullerene Cage. *J. Am. Chem. Soc.* **2015**, *137*, 7502−7508.
(32) van Eis, M. J.; Alvarado, R. J.; Echegoyen, L.; Seiler, P.; Diederich, F. First tether-directed regioselective bis-functionalisation of C: effects of cation complexation on the redox properties of diastereoisomeric fullerene crown ether conjugates. *Chem. Commun.* **2000**, 1859−1860.
(33) Brotsman, V. A.; Ioffe, I. N.; Troyanov, S. I. Crippling the C_{70} fullerene: non-classical $C_{68}Cl_{26}(OH)_2$ and $C_{68}Cl_{25}(OH)_3$ with three heptagons and only fused pentagons via chlorination-promoted skeletal transformations. *Chem. Commun.* **2022**, *58*, 6918−6921.
(34) Chen, H.; Xia, Z.; Miao, Q. Synthesis, aromatization and cavitates of an oxanorbornene-fused dibenzo[de,qr]tetracene nanobox. *Chem. Sci.* **2022**, *13*, 2280−2285.
(35) Purba, P. C.; Maity, M.; Bhattacharyya, S.; Mukherjee, P. S. A Self-Assembled Palladium(II) Barrel for Binding of Fullerenes and Photosensitization Ability of the Fullerene-Encapsulated Barrel. *Angew. Chem., Int. Ed.* **2021**, *60*, 14109−14116.
(36) Meng, W.; Breiner, B.; Rissanen, K.; Thoburn, J. D.; Clegg, J. K.; Nitschke, J. R. A Self-Assembled M_8L_6 Cubic Cage that Selectively Encapsulates Large Aromatic Guests. *Angew. Chem., Int. Ed.* **2011**, *50*, 3479−3483.
(37) Martínez-Agramunt, V.; Eder, T.; Darmandeh, H.; Guisado-Barrios, G.; Peris, E. A Size-Flexible Organometallic Box for the Encapsulation of Fullerenes. *Angew. Chem., Int. Ed.* **2019**, *58*, 5682−5686.
(38) Bobylev, E. O.; Poole, D. A., III; de Bruin, B.; Reek, J. N. H. M_6L_{12} Nanospheres with Multiple C_{70} Binding Sites for $^1O_2$ Formation in Organic and Aqueous Media. *J. Am. Chem. Soc.* **2022**, *144*, 15633−15642.

https://doi.org/10.1021/jacs.3c10808
J. Am. Chem. Soc. 2024, 146, 5186−5194

(39) Wietor, J.-L.; Pantoş, G. D.; Sanders, J. K. M. Templated Amplification of an Unexpected Receptor for C_{70}. *Angew. Chem., Int. Ed.* **2008**, *47*, 2689−2692.
(40) Kawano, S.-i.; Fukushima, T.; Tanaka, K. Specific and Oriented Encapsulation of Fullerene C_{70} into a Supramolecular Double-Decker Cage Composed of Shape-Persistent Macrocycles. *Angew. Chem., Int. Ed.* **2018**, *57*, 14827−14831.
(41) Yamashina, M.; Yuki, T.; Sei, Y.; Akita, M.; Yoshizawa, M. Anisotropic Expansion of an M_2L_4 Coordination Capsule: Host Capability and Frame Rearrangement. *Chem.—Eur. J.* **2015**, *21*, 4200−4204.
(42) Zhang, C.; Wang, Q.; Long, H.; Zhang, W. A Highly C_{70} Selective Shape-Persistent Rectangular Prism Constructed through One-Step Alkyne Metathesis. *J. Am. Chem. Soc.* **2011**, *133*, 20995−21001.
(43) Mulla, K.; Shaik, H.; Thompson, D. W.; Zhao, Y. TTFV-Based Molecular Tweezers and Macrocycles as Receptors for Fullerenes. *Org. Lett.* **2013**, *15*, 4532−4535.
(44) García-Simón, C.; Garcia-Borràs, M.; Gómez, L.; Parella, T.; Osuna, S.; Juanhuix, J.; Imaz, I.; Maspoch, D.; Costas, M.; Ribas, X. Sponge-like molecular cage for purification of fullerenes. *Nat. Commun.* **2014**, *5*, 5557.
(45) Xu, Y.; Kaur, R.; Wang, B.; Minameyer, M. B.; Gsänger, S.; Meyer, B.; Drewello, T.; Guldi, D. M.; von Delius, M. Concave-Convex π-π Template Approach Enables the Synthesis of [10]-Cycloparaphenylene-Fullerene [2]Rotaxanes. *J. Am. Chem. Soc.* **2018**, *140*, 13413−13420.
(46) Xu, Y.; von Delius, M. The Supramolecular Chemistry of Strained Carbon Nanohoops. *Angew. Chem., Int. Ed.* **2020**, *59*, 559−573.
(47) Lavendomme, R.; Jabin, I. Iteroselectivity, the missing sibling of chemo-, regio-, and stereoselectivities. *Cell Rep. Phys. Sci.* **2022**, *3*, 101121.
(48) García-Simón, C.; Colomban, C.; Çetin, Y. A.; Gimeno, A.; Pujals, M.; Ubasart, E.; Fuertes-Espinosa, C.; Asad, K.; Chronakis, N.; Costas, M.; Jiménez-Barbero, J.; Feixas, F.; Ribas, X. Complete Dynamic Reconstruction of C_{60}, C_{70}, and $(C_{59}N)_2$ Encapsulation into an Adaptable Supramolecular Nanocapsule. *J. Am. Chem. Soc.* **2020**, *142*, 16051−16063.

https://doi.org/10.1021/jacs.3c10808
J. Am. Chem. Soc. 2024, 146, 5186−5194